Exploring the oxidation and iron binding profile of a cyclodextrin encapsulated quercetin complex unveiled a controlled complex dissociation through a chemical stimulus

Dimitrios A. Diamantis[1], Sarka Ramesova[2], Christos M. Chatzigiannis[1], Ilaria Degano[3], Paraskevi S. Gerogianni[4], Constantina Karadima[6], Sonia Perikleous[6], Dimitrios Rekkas[6], Ioannis P. Gerothanassis[1], Dimitrios Galaris[4], Thomas Mavromoustakos[5], Georgia Valsami[6], Romana Sokolova[2*], Andreas G. Tzakos[1*]

[1]Department of Chemistry, Section of Organic Chemistry and Biochemistry, University of Ioannina, Ioannina 45110, Greece, agtzakos@gmail.com

[2]J. Heyrovský Institute of Physical Chemistry of the Czech Academy of Sciences, Dolejškova 3, 18223 Prague, Czech Republic, romana.sokolova@jh-inst.cas.cz

[3]Department of Chemistry and Industrial Chemistry, University of Pisa, Via Moruzzi 13, 56124 Pisa, Italy

[4]Laboratory of Biological Chemistry, University of Ioannina, School of Health Sciences, Faculty of Medicine, 451 10 Ioannina, Greece

[5]Department of Chemistry, National and Kapodistrian University of Athens, Panepistimiopolis Zografou 15771, Greece

[6]Department of Pharmacy, National and Kapodistrian University of Athens, Panepistimiopolis Zografou 15771, Greece

ABSTRACT

Background

Flavonoids possess a rich polypharmacological profile and their biological role is linked to their oxidation state protecting DNA from oxidative stress damage. However, their bioavailability is hampered due to their poor aqueous solubility. This can be surpassed through encapsulation to supramolecular carriers as cyclodextrin (CD). A quercetin- 2HP-β-CD complex has been formerly reported by us. However, once the flavonoid is in its 2HP-β-CD encapsulated state its oxidation potential, its decomplexation mechanism, its potential to protect DNA

damage from oxidative stress remained elusive. To unveil this, an array of biophysical techniques was used.

Methods

The quercetin-2HP-β-CD complex was evaluated through solubility and dissolution experiments, electrochemical and spectroelectrochemical studies (Cyclic Voltammetry) UV-Vis spectroscopy, HPLC-ESI-MS/MS and HPLC-DAD, fluorescence spectroscopy, NMR Spectroscopy, theoretical calculations (density functional theory (DFT)) and biological evaluation of the protection offered against H_2O_2 -induced DNA damage.

Results

Encapsulation of quercetin inside the supramolecule's cavity enhanced its solubility and oxidation profile is retained in its encapsulated state. Although the protective ability of the quercetin-2HP-β-CD complex against H_2O_2 was diminished, iron serves as a chemical stimulus to dissociate the complex and release quercetin.

Conclusions

We found that in a quercetin-2HP-β-CD inclusion complex quercetin retains its oxidation profile similarly to its native state, while iron can operate as a chemical stimulus to release quercetin from its host cavity.

General Significance

The oxidation profile of a natural product once it is encapsulated in a supramolecular cyclodextrin carrier as also it was discovered that decomplexation can be triggered by a chemical stimulus.

Highlights

- In-depth exploration of quercetin-2HP-βCD complex
- Electrochemical oxidation profile of quercetin inside the cavity of 2HP-βCD
- Iron triggers the decomplexation of quercetin from the cavity of 2HP-βCD
- DNA protection against oxidative stress induced from H_2O_2 from quercetin -2HP-βCD

KEYWORDS: Antioxidants, Metal complexes, Oxidation mechanism, Spectroelectrochemistry, quercetin, DNA protection

Abbreviations: Que: Quercetin, 2HP-β-CD: 2-hydroxypropyl-β-cyclodextrin, NMR: Nuclear Magnetic Resonance, UV-Vis: Ultraviolet visible. CD: Cyclodextrin.

1. Introduction

Natural products, also known as secondary metabolites, have served as a rich reservoir for the generation of potential drugs and their polypharmacological activity has been extensively explored [1]. Almost half of the FDA approved drugs over the last three decades originated from natural products [2]. Among them, flavonoids present an intriguing class of chemotypes bearing multifunctional biological activities.

Quercetin is a widely exploited flavonoid due to its diverse benefits in human health [3-5]. Its biological role is linked to its oxidation state protecting DNA from oxidative stress damage. Along these lines, the electrochemical oxidation of quercetin and other flavonols was intensively studied [6-10]. The first oxidation site is located at hydroxyl groups at the ring B (Fig. 1) and two-electron and two-proton oxidation is described by ECEC reaction mechanism (Electrochemical reaction – Chemical reaction - Electrochemical reaction – Chemical reaction). As the result of this complicated oxidation process is the formation of a benzofuranone derivative. The phenolic hydroxyl groups of ring A are oxidized in the second oxidation wave [7-10].

Although the diverse polypharmacological potential of quercetin, its use is limited due to its low aqueous solubility and thus, its low bioavailability [11]. To enhance its bioavailability, it is necessary to develop formulations with hosts like calixarenes, cyclodextrins, nanogels etc. Cyclodextrins (CDs) are supramolecules that can host in their cavities a variety of guest-molecules. Due to their toroidal shape, there is an internal hydrophobic side that traps the guest molecules while their external side is hydrophilic, thus enhancing water solubility and bioavailability [12, 13]. CDs have been utilized for a wide range of applications to surmount limitations such as poor solubility, bioavailability, plasma stability, metabolic inactivation etc

[14]. Another application is their use as Drug Delivery Systems (DDS) to avoid ectopic delivery and undesirable side effects to normal tissue. Such complexes were developed to enhance the bioavailability and aqueous solubility of the anti-inflammatory drug Naproxen for colon targeted delivery [15]. In another study, the complex formation between β-CD and 2-aminodiphenylamine (ADPA) was reported to confirm the expediency of its further application for the design of supramolecular nanovalves on the external surface of mesoporous silica particles [16]. Recently, a complex of silibinin with 2HP-β-CD that led to the enhancement of the aqueous solubility and a 10 fold increase of oral bioavailability compared to the parent compound was reported [17, 18]. Selective release of the guest molecule from the host can be triggered through different stimulus, though this is not trivial to be identified [19-22]. Although intense research is devoted for CD mediated inclusion complexes several critical points remain elusive. For instance, what are the chemical stimulus that can trigger the decomplexation of such complexes? In the case of flavonoids that their activity is linked to their oxidation potential it is not clear if their oxidation profile or metal ion binding profile is altered once they are encapsulated in a supramolecular carrier. Also, questions exist on the capability of such inclusion complexes to protect DNA from oxidative damage. To resolve these issues an array of biophysical techniques was applied on the inclusion complex of quercetin with 2HP-β-CD [23]. Herein is described an intensive exploration of the oxidative profile of quercetin once is in the cavity of the CD host as also its metal ion binding profile, its DNA protection behavior against oxidative stress conditions and a chemical stimulus was revealed that can lead to a controlled release of the flavonoid from the host core. Such information could allow exploiting the untapped potential that can be offered for natural products implicated in host-guest complexes.

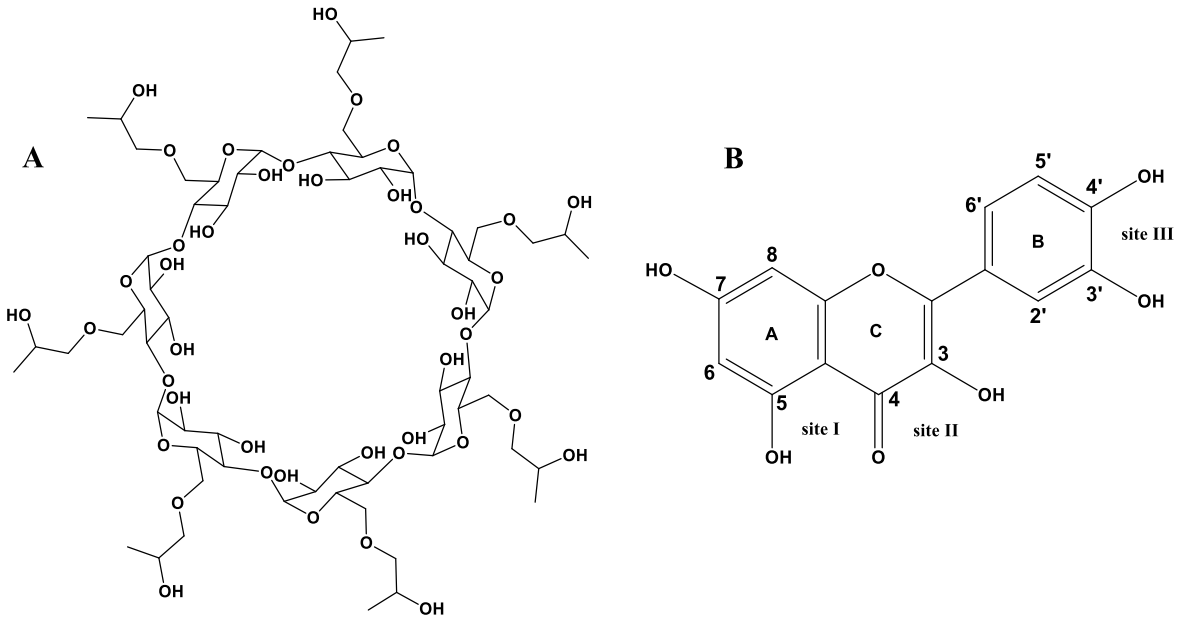

***Figure 1**: (A) Structure of 2HP-β-CD and (B) Structure of quercetin and the 3 possible binding sites (I-III) for metal ion chelation.*

2. Materials and methods

2.1 Complex preparation

The lyophilized complex of quercetin with 2HP-β-CD (Que-2HP-β-CD) was prepared as previously described using a freeze-drying procedure [14]. Briefly, Que-2HP-β-CD aqueous solutions for freeze-drying were prepared in a molar ratio of 1:2, using the neutralization method. More specifically, 0.030 g of Que and 0.306 g of 2HP-β-CD were weighed accurately, transferred in a 50 mL beaker and suspended with 20 mL of water. Small amounts of ammonium hydroxide were then added under continuous stirring and pH monitoring until complete dissolution and pH adjustment to a value between 9 and 10 has been obtained. The resulting solution at molar ratio of 1:2 was thereafter frozen at -80 ^{o}C and freeze-dried using a Kryodos-50 model Telstar lyophilizer.

2.2 Solubility studies and Dissolution experiments

Solubility studies for Que and the Que-2HP-β-CD lyophilized product were performed using a thermostated shaking bath (Unitronic orbital J.P. Selecta) with adapted thermostating unit, while a Shimadzu UV-1700 Pharma Spec UV/VIS spectrometer was used for spectrophoto-

metric measurements. The aqueous solubilities of pure Que and Que obtained from the lyophilized Que-2HP-β-CD product were measured at pH 1.2, 4.5 and 6.8 at 37 ^{o}C as described in the relevant guidelines of both the European Medicines Agency (EMA) [24] and the American Food and Drug Administration (FDA) [25]. Specifically, an excess amount of Que or Que-2HP-β-CD lyophilized product was added to 10 mL of either HCl solution pH 1.2 or acetate buffer pH 4.5 or phosphate buffer 6.8. After equilibration for 0, 3, 6, 15, 24 and 48 h at the thermostated shaking bath (37 ± 0.5 ^{o}C, 50 rpm) suspensions were filtered through regenerated cellulose syringe filters of 0.45 μm pore size and the Que concentration was determined spectrophotometrically after dilution with mixed MeOH-aqueous medium solution (50:50 v/v).

Dissolution experiments for Que and Que-2HP-β-CD lyophilized product were performed using a USP dissolution apparatus II (Erweka DT6 Dissolution Tester). All experiments were performed in triplicate at pH 1.2, 4.5 and 6.8, at 37 ^{o}C and 100 rpm. An accurately weighed amount of Que or an equivalent amount of the lyophilized Que-2HP-β-CD product was placed into an empty capsule (in triplicate). The filled capsules were placed in the vessels of a USP dissolution apparatus II (Erweka DT6 Dissolution Tester) and were kept at the bottom with the help of metal spirals. The dissolution medium was 500 mL of either HCl pH 1.2 or acetate buffer pH 4.5 or phosphate buffer pH 6.8 and dissolution was performed at 37 ± 0.5 ^{o}C and at 100 rpm rotation speed. Samples (2.5 mL) were withdrawn at appropriate time intervals (5, 10, 15, 20, 30, 45, 60, 120 and 180 min) after the beginning of the experiment, they were filtered through regenerated cellulose syringe filters (pore size 0.45 μm), and were assayed spectrophotometrically for Que.

2.3 Electrochemical and spectroelectrochemical studies

In electrochemical measurements, potassium chloride, and chemicals for preparation of Britton-Robinson buffers (0.04 mol·L^{-1} stock solutions of H_3PO_4, CH_3COOH, H_3BO_3 and 0.2 mol·L^{-1} NaOH, Sigma Aldrich), which were used as supporting electrolytes, were of reagent grade. The solutions were prepared with Millipore ultrapure water. Ethanol was present in solution in the ratio 40% (*v*/*v*) to increase quercetin solubility and did not affect the stability of 2HP-βCD complex.

Cyclic voltammetry was measured in a three-electrode system with Ag|AgCl|1M LiCl reference electrode separated from the examined solution by a salt bridge, glassy carbon working electrode (diameter 0.7 mm) and platinum net as the auxiliary electrode using a PGSTAT 12 AUTOLAB potentiostat (Ecochemie, Utrecht, NL). The spectroelectrochemical measurements were performed in an optically transparent thin-layer electrode (OTTLE) cell [26] with a three-electrode system (Ag/AgCl reference electrode) mounted in a thin layer (thickness 0.18 mm) between optical windows (CaF_2). A sufficiently optically transparent platinum gauze (5×5 mm size, 80 mesh) was used as the working electrode. The scan rate was 5 $mV \cdot s^{-1}$. Absorption spectra during the electrolysis were registered using an Agilent 8453 diode-array UV-Vis spectrometer. The oxidation products of 2HP-βCD complex prepared by the exhaustive oxidative electrolysis at a carbon paste electrode were identified by HPLC-ESI-MS/MS and HPLC-DAD.

HPLC-DAD analyses were performed on a Jasco International Co., Japan system composed by a PU-2089 Quaternary Gradient Pump with degasser, with an AS-950 auto-sampler and a photo-diode array detector MD-2010. Data acquisition and analysis were performed by ChromNav® software. The separation was performed on an analytical reverse phase Agilent TC-C18(2) column (150x4.6 mm, 5 μm particle size) connected to a precolumn C-18 (12.5x4.6 mm, 5 μm particle size). The programme was: 85% A (bidistilled water with 0.1% trifluoroacetic acid) and 15% B (LC grade acetonitrile with 0.1% trifluoroacetic acid) for 5 min, then 25 min gradient from 85% A to 50% A, then 10 min gradient from 50% A to 30% A, then 1 min gradient from 30% A to 0% A and then 5 min cleaning (100% B) and 10 min re-equilibrating time (85% A). The flow rate was 1 $mL \cdot min^{-1}$. The injection volume was 20 μL. DAD spectra were acquired with 4 nm resolution in the range 200-650 nm.

HPLC-ESI-MS/MS analyses were performed on an Agilent Technologies, USA 1200 Infinity HPLC, coupled to a Quadrupole-Time of Flight tandem mass spectrometer 6530 Infinity Q-TOF through a Jet Stream ESI interface. The separation took place at 30 °C and was performed on a Zorbax Extend C18 Rapid resolution HT column (50x2.1 mm, 1.8 μm particle size), with a Zorbax Eclipse Plus C18 Analytical Guard Colum. The programme was: 90% A (LC-MS grade water with 1% formic acid) and 10% B (LC-MS grade acetonitrile with 1% formic acid) for 2 min, then to 50% A in 9 min, then linear gradient to 30% A in 3 min, then to 10% A in 4 min, re-equilibration took 3 min. The flow rate was 0.2 $mL \cdot min^{-1}$. The injec-

tion volume was 10 μL. The operating conditions of the ESI interface were: drying gas N_2 (purity >98%) at 350 °C and 10 $L \cdot min^{-1}$; sheath gas N_2 (purity >98%): 375 °C and 11 $L \cdot min^{-1}$, capillary voltage at 4.5 kV; nebulizer gas 35 psig. The fragmentor was operated at 175 V. High resolution MS and MS/MS spectra were acquired in negative mode in the range 100-3200 *m*/*z* and the voltage applied in the collision cell for the MS/MS experiments ranged between 20 and 50 V. Collision gas was nitrogen (purity 99.999%). The mass axis was calibrated daily using the Agilent tuning mix HP0321 prepared in acetonitrile.

2.4 UV-Vis spectroscopy

The UV-Vis spectra of Que-2HP-β-CD complex were recorded with a Perkin Elmer Lambda 25 spectrometer (slit=1, speed 240 nm/min) at room temperature. The samples were dissolved in LC-MS grade H_2O, pH was adjusted to 7.25 and 5.81 by the addition of aqueous solution of 10 $mmol \cdot L^{-1}$ NaOH and 10 $mmol \cdot L^{-1}$ HCl and incubated under shaking at 37 ± 0.1 ^oC at 600 rpm using thermostated shaking bath for the proper time period. Then the samples were centrifuged at 10.000 rpm for 5 minutes and the precipitated Que was filtered off through regenerated cellulose syringe filters of 0.20 μm pore size. Typical titration experiments were performed by sequential addition/ns of freshly prepared metal ion solutions (30 $mmol \cdot L^{-1}$ stock solution, freshly prepared in double distilled water) to the same 3 mL sample solution (17.5 $\mu mol \cdot L^{-1}$) in a quartz cuvette.

2.5 Fluorescence spectroscopy

The fluorescence spectra of Que-2HP-β-CD (17.0 μM) were recorded at a JASCO FP-8000 Fluorimeter (slit=5, excitation at 370 nm). Typical titration experiments were performed by sequential additions of freshly prepared metal ion solutions (30 $mmol \cdot L^{-1}$ stock solution, freshly prepared in double distilled water) to the same 3 mL sample solution (17.5 $\mu mol \cdot L^{-1}$) in a quartz cuvette.

2.6 NMR Spectroscopy

^{1}H-NMR spectra of Que-2HP-β-CD complex and 2HP-β-CD were recorded in a Bruker 400 MHz Avance spectrometer using D_2O and DMSO-d_6 as solvent. Samples were dissolved in 500μL D_2O and transferred to 5 mm NMR tubes. Topspin 3.1 was used to control the NMR system. Typical titration experiments were performed by sequential additions of freshly prepared metal ion solution in D_2O (246.25 mmol·L^{-1} stock solution) to the same sample solution (3.8 mmol·L^{-1}) in an NMR tube.

2.7 Theoretical calculations

Molecular orbital calculations were performed using the density functional theory (DFT) employing B3LYP functional and 6-31G* basis set in the environment of Spartan '14, v.1.1.0. (Wavefunction, Inc.) for the Que-2HP-β-CD complex in vacuum.

2.8 Cell cultures

RPMI-1640 growth medium supplemented with L-glutamine and glucose oxidase (from Aspergillus niger, 18,000 units/g) were obtained from Sigma-Aldrich (St. Louis, MO, USA). Fetal bovine calf serum (FBS), Nunc tissue culture plastics, low melting-point agarose and penicillin/ streptomycin antibiotics were obtained from Gibco GRL (Grand Island, NY, USA). Microscope superfrosted glass-slides were supplied by Menzel-Glaset (Menzel, Germany).

Cell cultures Jurkat cells (ATCC, clone E6-1) were grown in RPMI-1640 containing 10% heat-inactivated FBS, 2mM glutamine, 100 U/ml penicillin and 100ng/ml streptomycin, at 37°C in 95% air and 5% CO_2. Jurkat cells in the log phase were harvested by centrifugation (250g, 10min), resuspended at a density of 1.5×10^6 cells per ml and allowed to stay for 1h under standard culturing conditions before treatments.

2.9 Evaluation of the protection offered against H_2O_2 -induced DNA damage

Cells were treated with each compound for the time periods indicated under otherwise standard culture conditions and then exposed for 10 min to continuously generated H_2O_2 formed

by the action of the enzyme "glucose oxidase" which was added directly to the growth medium. The amount of the enzyme added was estimated to generate approximately 10μM of H_2O_2 per min. Cells were then collected and analyzed for the formation of single strand breaks in their DNA by comet assay.

The alkaline comet assay was performed essentially as described previously by Singh *et al*.[27] with minor modifications [28]. In brief, cells were suspended in 1% (w/v) low-melting-point agarose in PBS, pH 7.4, and pipetted onto superfrosted glass microscope slides, precoated with a layer of 1% (w/v) normal melting-point agarose (warmed to 37°C prior to use). The agarose was allowed to set at 4°C for 10min, and the slides were then immersed for 1h at 4°C in a lysis solution (2.5M NaCl, 100mM EDTA, 10mM Tris, pH 10, 1% Triton X-100) in order to dissolve cellular proteins and lipids. Slides were placed in single rows in a 30cm-wide horizontal electrophoresis tank containing 0.3M NaOH and 1mM EDTA, pH ~ 13 (unwinding solution) and kept at 4°C for 40min in order to allow DNA strand separation (alkaline unwinding). Electrophoresis was performed for 30min in the unwinding solution at 30V (1V/cm) and 300mA. Finally, the slides were washed for 3 × 5min in 0.4M Tris (pH 7.5, 4°C) and stained with Hoechst 33342 (10mg/ml). Hoechst-stained nucleoids were examined under a UV-microscope with a 490nm excitation filter at a magnification of ×400. DNA damage was not homogeneous, and visual scoring was based on the characterization of 100 randomly selected nucleoids, as previously described [28]. In brief, the comet-like DNA formations were categorized into five classes (0, 1, 2, 3 and 4) representing an increasing extent of DNA damage visualized as a 'tail'. Each comet was assigned a value according to its class. Accordingly, the overall score for 100 comets ranged from 0 (100% of comets in class 0) to 400 (100% of comets in class 4). In this way the overall DNA damage of the cell population can be expressed in arbitrary units.

3. Results and discussion

3.1 Solubility and dissolution studies

For orally administered drugs and especially low aqueous soluble drugs as Que, aqueous solubility, in conjunction to their rate of dissolution, and intestinal permeability are the main pa-

rameters controlling the rate and extent of gastrointestinal absorption and consequently oral bioavailability [29]. The aqueous solubility and dissolution characteristics of the prepared Que-2HP-β-CD lyophilized product in comparison to that of the parent Que were studied, at the physiological gastrointestinal pH range, recommended in the relevant FDA and EMA guidelines [24, 25].

The results from the solubility studies for both pure Que and the Que-2HP-β-CD complex are presented in Fig. 2A and Fig. 2B. In order to probe the amplification offered on quercetin's aqueous solubility in its encapsulated form with CD detailed solubility studies were conducted at pH 1.2, 4.5 and 6.8 according to the relevant FDA and EMA guidelines [24, 25]. These pH values could be interpreted on the basis of gastrointestinal absorption after oral drug administration, since, under fasting conditions, the pH range in the GI tract vary from 1.4 to 2.1 in the stomach, 4.9 to 6.4 in the duodenum, 4.4 to 6.6 in the jejunum, and 6.5 to 7.4 in the ileum [30-32]. UV assay revealed 8% w/w content of Que in the Que-2HP-β-CD complex. The solubility of pure Que ranged from 0.004±0.002 mg/mL at pH 1.2 and 4.5 to 0.016±0.001 mg/mL at pH 6.8. The solubility of the lyophilized Que-2HP-β-CD complex was reached maximum at early times at all pH values studied and declined gradually to lower values at the 24^{th} and 48^{th} hour of the experiment probably due to either Que-2HP-β-CD complex decomposition or initial formation of supersaturated solution and gradual transition to the stable saturated form at later time points. More specifically, the measured Que solubility was found 0.19±0.07 mg/mL at pH 1.2, 0.13±0.2 mg/mL at pH 4.5 and 0.47±0.117 mg/mL at pH 6.8. These values remained constant for 3h (pH 6.8) to 15h (pH 1.2 and 4.5) and declined to 0.07±0.04 mg/mL at pH 1.2, 0.085±0.004 mg/mL at pH 4.5 and 0.23±0.03 mg/mL at pH 6.8, after 24h. It is obvious that the interaction of Que with 2HP-β-CD resulted in the increase of Que's solubility with a solubilization effect, as reflected on Que-2HP-β-CD to Que solubility ratio, higher than 10 in all pH studied (Table 1). From the results presented in Table 1 it is evident that Que inclusion in the cavity of 2HP-β-CD resulted in 47 to 17 times increase of solubility at pH 1.2, 32 to 21 times increase of solubility at pH 4.5 and 29 to 14 times increase of solubility at pH 6.8.

Table 1: *Measured solubility (Cs) of parent Que and Que from the Que-2HP-β-CD lyophilized product at pH 1.2, 4.5 and 6.8*

	pH	Cs (mg/ml) ± SD	Que-2HP-β-CD to Que solubility ratio	D_0=Dose/(Cs×V)[g]
QUE	1.2	0.004±0.001[a]	-	32.4
	4.5	0.004±0,001[b]	-	32.4
	6.8	0.016±0.004[c]	-	8.1
QUE-HP-β-CD	1.2	0.19±0.07[b] – 0.07±0.04[d]	47.5 – 17.5	0.682 – 1.85
	4.5	0.13±0.02[b] - 0.085±0.004	32.5 – 21.25	0.996 – 1.52
	6.8	0.47±0.117[e] – 0.23±0.03[f]	29.4 – 14.4	0.276 – 0.563

[a] mean ± SD from all concentration measurements, [b] concentrations measured (mean ± SD) at 3, 6 and 15 h of experiment, [c] concentration measured (mean ± SD) at 48 h of experiment, [d] concentration measured (mean ± SD) at 24 and 48 h of experiment, [e] concentration measured (mean ± SD) at 3 h of experiment, [f] concentration measured (mean ± SD) at 15, 24 and 48 h of experiment; g Dose= 32.4 mg [33]

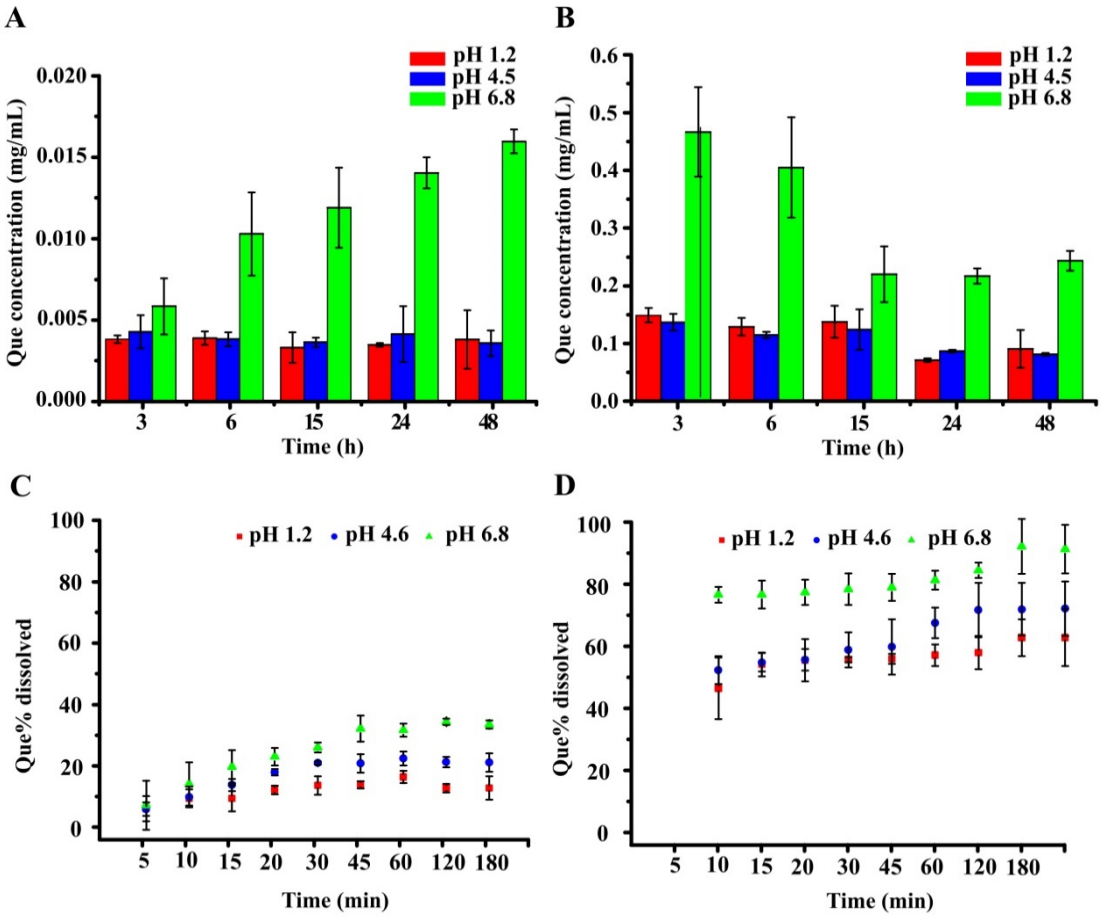

Figure 2: *Effect of pH on the solubility of (A) pure Que and (B) the Que-2HP-β-CD lyophilized complex and on the dissolution of (C) pure Que and (D) the Que-2HP-β-CD lyophilized complex.*

The results from the dissolution studies are shown in Fig. 2C and 2D for both the pure Que and the Que-2HP-β-CD lyophilized product at pH 1.2, 4.5 and 6.8. The amount of pure Que dissolved ranged from 10.3±3.8% w/w at pH 1.2 to 18.7±3.1% w/w at pH 4.5 and 31.1±1.5% w/w at pH 6.8. These values correspond to the final concentration of Que in the dissolution medium of 0.007, 0.004 and 0.012 mg/ml at pH 1.2, 4.5 and 6.8, respectively and are consistent with the results from the solubility study for pure Que. Considering the dissolution of the Que-2HP-β-CD lyophilized product was 3 to 6 times higher than that of pure Que at pH ranging from 1.2 to 6.8. More specifically, Que was completely dissolved at pH 6.8 (90.4±8.8% w/w) from its Que-2HP-β-CD lyophilized product, while 70.4±9.8% w/w and 61.1±9.2% w/w dissolution was observed at pH 4.5 and 1.2, respectively, during the three hours of the dissolution experiments. These results confirm the solubilizing effect of 2HP-β-CD on Que and are consistent with the observed solubility values for the Que-2HP-β-CD lyophilized product (Table 1, Fig. 2).

Adopted by both FDA and EMA and described in the relevant regulations on waiver of *in vivo* bioavailability and bioequivalence studies and investigation of bioequivalence, respectively [24, 25], the Biopharmaceutics Classification System (BCS) [34] consists a scientific framework for classifying drug substances into four classes based on their aqueous solubility and gastrointestinal permeability, using the highest dose within the physiologically relevant range of pH 1−6.8, as follows: Class I: High Solubility – High Permeability, Class II: Low Solubility – High Permeability, Class III: High Solubility – Low Permeability, Class IV: Low Solubility – Low Permeability.

Recently, Waldaman *et al.* [34], presented a provisional BCS classification strategy for herbal markers according to the available information. Quercetin, one of the markers of Gingko biloba, was classified in Class IV, characterized by both low solubility and permeability, in agreement with the reported low bioavailability of Que [11]. Using the same Classification Criteria as Waldman *et al* [34] the dose number (D_0=Dose/(Cs*V)), which describes the rela-

tionship between solubility and maximum dose strength, for both Que and the Que-HP-β-CD lyophilized product was calculated, for V=250 mL and the measured Cs values at pH 1.2, 4.5 and 6.8 (Table 1). Compounds with a D_0 lower or equal to 1 are considered highly soluble [25, 35] and are classified in either Class I or Class III according to their permeability. It is obvious from the results in Table 1 that the Que-2HP-β-CD lyophilized product is classified as highly soluble in the entire physiologically relevant range of pH 1−6.8, while for Que D_0>1 was calculated in all cases. This, in conjunction to the rapid and almost complete dissolution observed, points out that the Que-2HP-β-CD lyophilized product has an increased bioavailability after oral administration.

3.2 Stability evaluation of the Que-2HP-β-CD complex in aqueous solution through UV-Vis

The UV-Vis spectra of most flavonoids consist two major absorption bands centered approximately at 260 nm and 350 nm originating from the benzoyl and cinnamoyl bands, respectively and can be assigned to HOMO-LUMO energy gaps and π-π* transitions [36].

Initially, the time-dependent oxidation profile of the Que-2HP-β-CD complex (39.5 $\mu mol \cdot L^{-1}$) in aqueous solution (pH=7.14) was monitored. As illustrated in Fig.3, the complex was stable for 3 hours and considerable alterations emerged after this time. The absorbance of the major bands at 370 nm and 257 nm gradually decreased with parallel shifting to 376 nm and 254 nm, respectively. On the other hand, the absorbance of the minor band at 288 nm gradually increased and red-shifted to 294 nm. The band at 294 nm is related to the decomposition of the oxidation product of quercetin (i.e. a benzofuranone derivative) and the formation of the main stable product, which is 3,4 dihydroxybenzoic acid, as demonstrated by HPLC-DAD and HPLC-ESI-MS analyses [10].

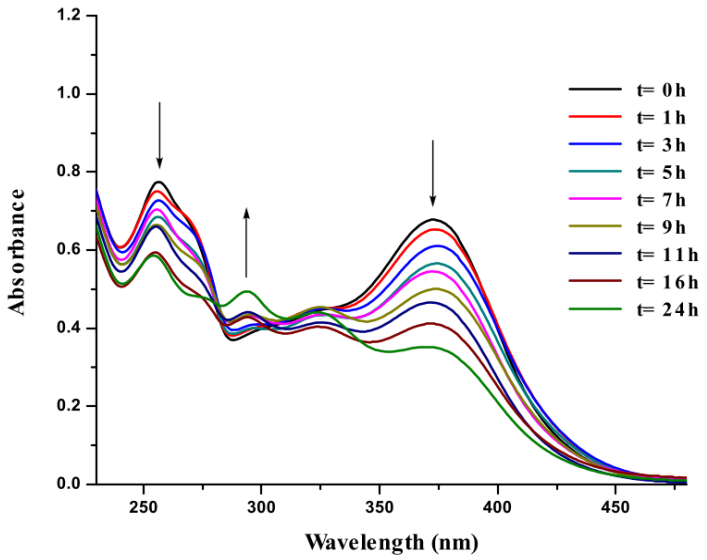

Figure 3: *Time-course UV-Vis absorption spectra of an aqueous solution of Que-2HP-β-CD complex (39.5μM) at pH 7.14.*

3.3 Mapping the oxidative state of quercetin in the CD encapsulated form via electrochemical and spectroelectrochemical studies

In order to evaluate the oxidation state of quercetin in its encapsulated form and whether this is altered to its free form electrochemical and spectroelectrochemical studies were utilized. This is of immense importance since such information, concerning the oxidative profile of a flavonoid once is in a CD formulation, is currently elusive. Cyclic voltammetry of Que-2HP-β-CD complex in solution at pH 4.3 and 7.6 showed three oxidation peaks labelled as I., II., and III., respectively (Fig. 4 A and B, respectively). The first two oxidation peaks at 0.36 V and 0.17 V were quasi reversible. The oxidation properties of the complex were in accordance with those of the free molecule of quercetin; a comparison of the free quercetin and its complexed form is illustrated in Fig. 4C and D for pH 8.8. The oxidation waves of the Que-2HP-β-CD complex are attributed to the oxidation of the hydroxyl groups located in ring B (labelled as I.) and occurred at all the investigated pH values at the same potential as in the case of free quercetin. Moreover, oxidation peaks II. (corresponding to the oxidation of a benzofuranone product formed at the potential of the first wave) and III. (assigned to the oxidation of hydroxyl groups at the ring A) were present in cyclic voltammograms of both com-

plexed and free forms of quercetin. Thus, all the electroactive sites of quercetin that are bound in the cavity are available. This fact agrees with the chemical structure of the complex, where ring B and carbon atoms C2 and C3 and keto group C4=O are available from one side of the cavity, and the hydroxyl groups of ring A are reachable from the other side (Fig.S1. The position of the molecule of quercetin in the cavity was confirmed by DFT theoretical calculations (Fig. S1). Resulting data are in the agreement with the electrochemical findings, that all three electroactive sites of quercetin are available even if complexed in cavity. Cyclic voltammograms in Fig. 4 C and D show an additional wave Ib, attributed to the one-electron oxidation of dianion A^{2-} present in solution at this pH, while Ia is the oxidation wave of the remaining anion AH^{-}. The oxidation properties were systematically investigated in Britton-Robinson buffers in the range of pH 4.0 – 9.8 (Fig. 5). Oxidation peaks were shifted to less positive values when pH was increased. The inset in Fig. 6 shows a dependence of peak potential on pH for oxidation waves attributed to the oxidation of the non-dissociated form of Que-2HP-β-CD complex and its anion. The intersection point of two linear segments yields the apparent dissociation constant pK' = 6.7, which is in agreement with the dissociation constant reported in the literature [10]. The complex was decomposed at pH higher than 8.8 and a decrease of currents was observed. The dependence of the peak current on the square root of the scan rate is linear and the oxidation process is thus diffusion controlled (Fig. S2 in Supporting information. Oxidation at the first oxidation wave involved two electrons and two protons, as confirmed by coulometry and from the slope of peak potential vs. pH dependence (inset in Fig. 5).

Comparison of the oxidation behavior of free quercetin and the Que-2HP-β-CD complex shows no differences. Quercetin retains its electrochemical properties when it is encapsulated to the cavity of 2HP-β-CD. It means, that all electroactive sites of quercetin are available in the cyclodextrin cavity and no significant differences were monitored between cyclic voltammetries of free and complexed quercetin. The potential of peak II. of Que-2HP-β-CD complex belonging to a product of oxidation is 54 mV lower than in case of free molecule (Fig. S2 in Supporting information). This implies that the oxidation product can be more easily oxidized while protected in cavity against moving from the electrode or its decomposition.

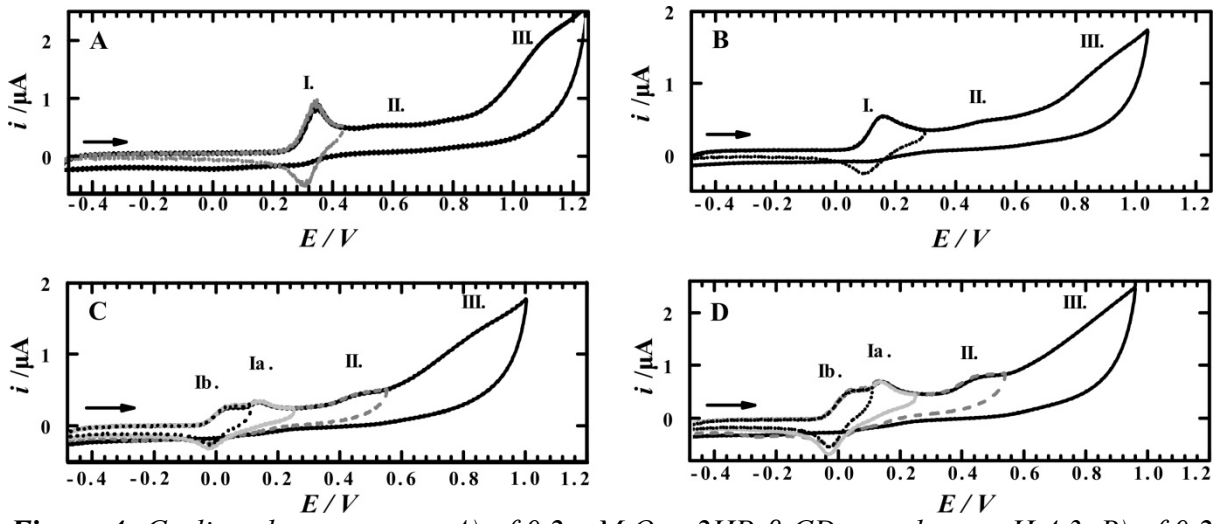

***Figure 4**: Cyclic voltammograms A) of 0.2 mM Que-2HP-β-CD complex at pH 4.3, B) of 0.2 mM Que-2HP-β-CD complex at pH 7.6, C) of 0.2 mM Que-2HP-β-CD complex at pH 8.8 and D) of 0.4 mM quercetin at pH 8.8.*

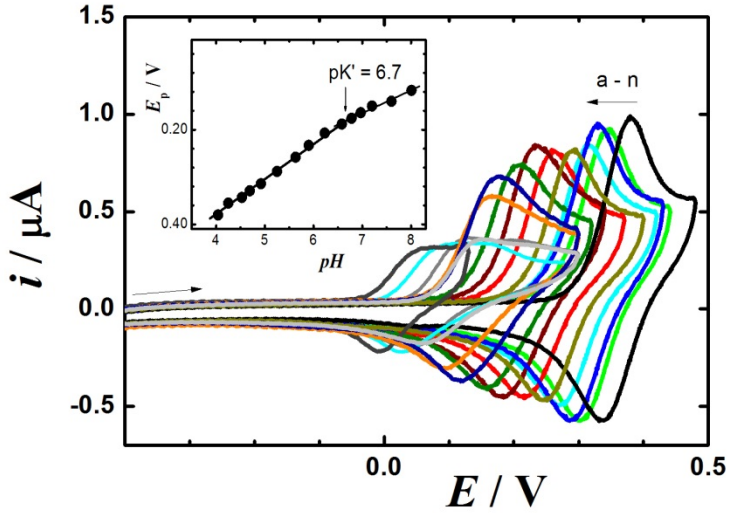

***Figure 5**: Selected cyclic voltammograms of 0.2 mM Que-2HP-β-CD complex at different pH values: (a) 4.0, (b) 4.5, (c) 4.7, (d) 4.9, (e) 5.3, (f) 5.6, (g) 5.9, (h) 6.2, (i) 6.8, (j) 7.0, (k) 7.2, (l) 8.0, (m) 8.2, (n) 8.8. Scan rate was 0.1 V·s^{-1}. Inset: Dependence of peak potential on pH (Pourbaix plot).*

The UV-Vis spectra were recorded also using *in situ* spectroelectrochemistry in an optically transparent thin-layer electrode cell. Spectroelectrochemistry at the potential of the first oxidation wave showed a decrease of the bands at 274 and 393 nm and simultaneous increase of the intensity at 333 nm (Fig. 6A). This process is characterized by a sharp isosbestic point at 365 nm. The resulting spectrum of intermediate changes as the oxidation proceeds, as pre-

sented in Fig. 6B. An increase of the absorption band at 295 nm accompanies the further decrease of bands at 393 and 333 nm. These findings support results obtained by cyclic voltammetry mentioned above. No significant difference in oxidation mechanism was found in the case of quercetin encapsulated in the cavity of 2HP-β-CD compared to free quercetin [10].

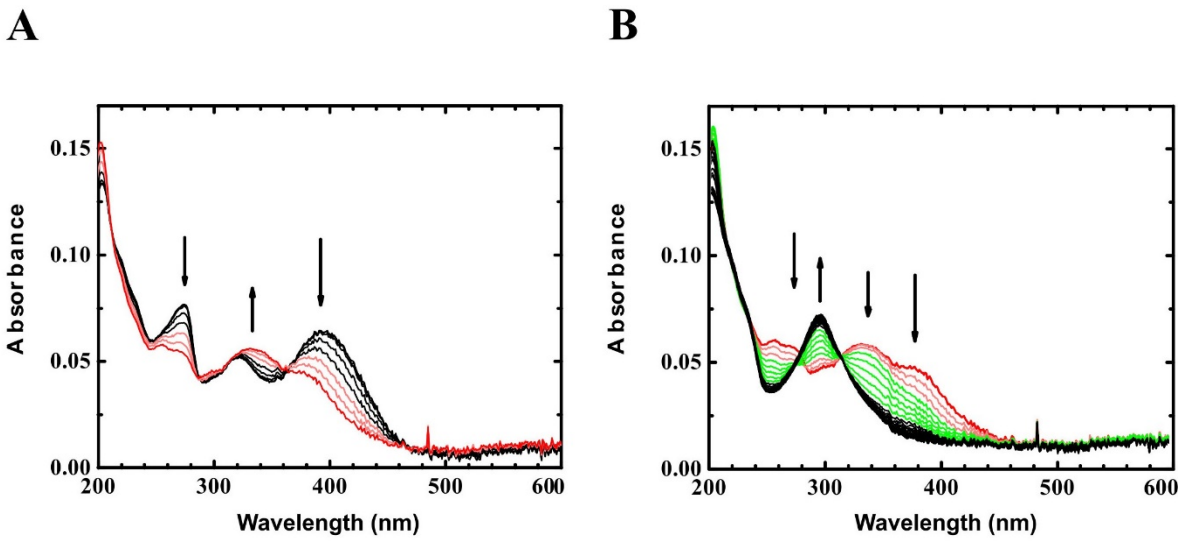

***Figure 6**: In situ spectroelectrochemistry of 0.2 mM Que-2HP-β-CD complex in 0.1 mol·L^{-1} KCl (A) at the edge of the first oxidation peak and (B) at the potential behind the first oxidation peak.*

The oxidation products of Que-2HP-β-CD complex after electrolysis at the potential of the first oxidation peak were also identified by HPLC-DAD and HPLC-ESI-MS/MS analysis (Table 2). The oxidation pathway led to the formation of two species (**P1** and **P2**), both with molecular ion $[M-H]^-$ corresponding to the raw formula $C_{14}H_8O_8$ indicative of the decomposition products of the semiquinone intermediate. These products were not identified in the study on the oxidation of free quercetin due to their short lifetime [10]. Two possible isomers can be formed from the opening of the semiquinone structure, as shown in Scheme 1. The UV-Vis spectrum acquired by DAD of the specie eluting later is characterised by absorption maxima at 265 and 360 nm, consistent with the UV-Vis spectroelectrochemistry results. The tandem mass spectra of both species are characterised by the presence of a fragment ion at 285.00, consistent with the loss of water. Moreover, 2,4,6-trihydroxybenzoic acid (**P3**) along

with 3,4-dihydroxybenzoic acid (**P4**) are present, which can be derived from the decomposition of **P1** and **P2**. Similar open structures were identified as minor oxidation products of flavonols in aqueous solutions, but they were derived from flavonol structure [8]. Compound **P3** has been described as the final oxidation product of quercetin in literature [37, 38]. In this case, the unique protection of the semiquinone intermediate by the cavity of 2HP-β-CD allowed identifying its presence by direct detection, and not through the interpretation of the oxidation pathway.

Table 2 *The oxidation products of Que-2HP-β-CD complex*

Species	Tr (min)	Assignment	Raw formula	$[M-H]^-$ m/z	product ions	λ_{max} (nm)
P3	1.3	2,4,6-trihydroxybenzoic acid	$C_7H_6O_5$	169.014	151.004, 125.025, 107.014	n.d. (eluting with the dead volume)
P4	1.5	3,4-dihydroxybenzoic acid	$C_7H_6O_4$	153.019	109.029	260, 295
P1	12.0	2-[(3,4-dioxocyclohexa-1,5-diene-1-carbonyl)oxy] -4,6-dihydroxybenzoic acid	$C_{14}H_8O_8$	303.014	285.001	n.d. (below limit of detection)
P2	16.0	3,4-dioxocyclohexa-1,5-dien-1-yl oxo(2,4,6-trihydroxyphenyl)acetate	$C_{14}H_8O_8$	303.016	285.005	265, 360

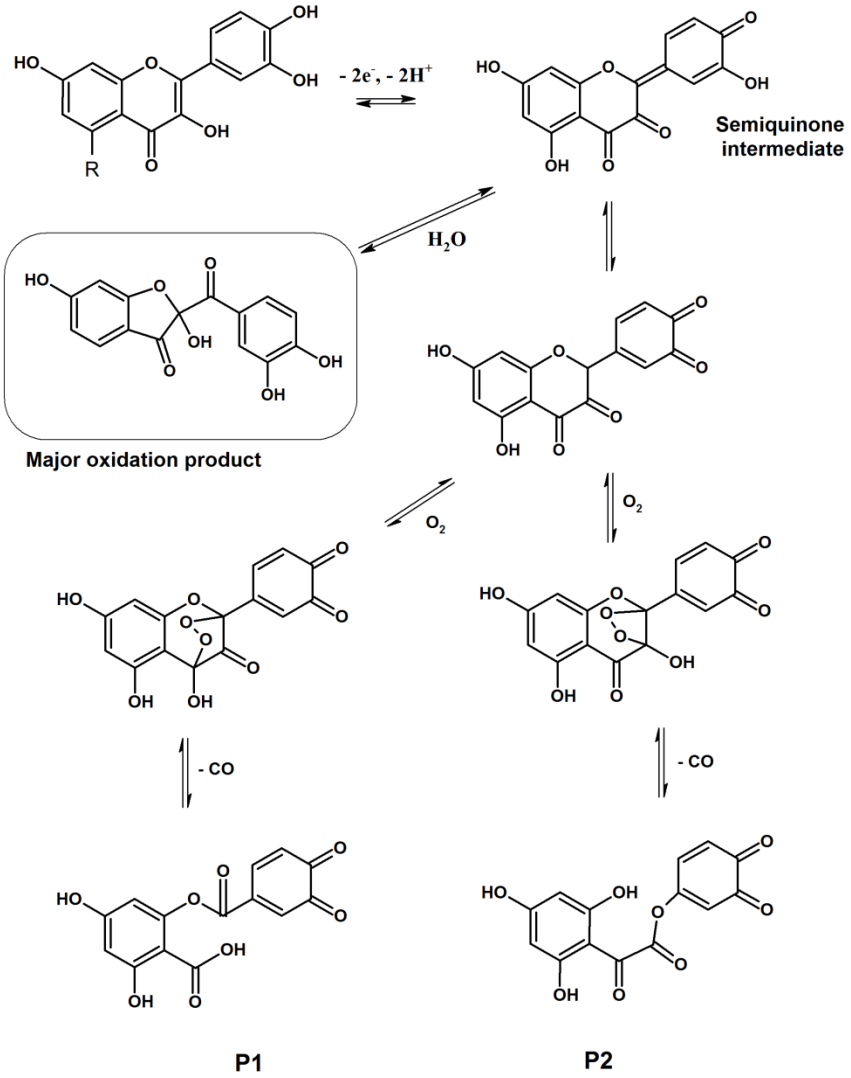

Scheme 1. *Suggested mechanism of oxidative decomposition of quercetin via a semiquinone intermediate.*

3.4 Charting the Fe2+ and Fe3+ binding profile of the encapsulated Quercetin unveiled chemical stimulus for a controlled dissociation of the 2HP-βCD – Quercetin complex

Although iron has been evolutionary selected as the main catalyst for biological redox reactions, once in its redox-active form, it can catalyze Fenton-type reactions generating extremely reactive free radicals that are harmful for cell [39]. Along these lines, several natural products can tailor the intracellular labile iron levels and determine the cell fate in conditions of elevated oxidative stress [40]. As it was recently reported, the potential of natural products to protect cells against H_2O_2-induced DNA damage and apoptosis is linked to their capacity to

chelate labile iron [41]. Along these lines it was set out to determine whether quercetin was able to retain its metal ion binding potential once it is in its encapsulated form to CD. This point, although of paramount importance also remained unknown to our knowledge, as it has never been evaluated before in any other antioxidants-CD encapsulated formulations.

Quercetin has the ability to chelate numerous metal ions in different binding sites [36, 42-46]. Metal chelation can take place up to three different sites on the quercetin scaffold (Fig. 1B): (i) on the 7-phenolic hydroxyl group - 4 keto group on rings A and C respectively, (ii) the 3-phenolic hydroxyl group - 4 keto group on ring C and (iii) the catechol group of ring B, influencing both the photochemical properties of quercetin and its biological activity. Flavonoids pro-oxidant effects have been directly correlated with their ability to bind metals like copper and iron and being affected by their reducing activities. Especially iron is present in various forms among the biological systems and its reducing properties during interaction with quercetin is of major significance [47].

Upon chelation with metal ions, the UV-Vis spectra of flavonoids change, displaying a bathochromic shift that can be attributed either to the reduced HOMO-LUMO gaps or to Ligand to Metal Charge Transfer (LMCT) [46, 48]. UV-Vis and fluorescence titrations of Que-2HP-β-CD inclusion complex (17 μM) with Fe^{2+} and Fe^{3+} were performed in aqueous solution at two different pH values (7.25 and 5.81). Three phenomena could co-exist upon iron titration: complexation of iron to Que or complexation of iron to cyclodextrin or both. As illustrated in Fig. 7A and 7B, it was found a decrease in the intensity of the major peak at 370 nm that depends on the amount of titrated Fe^{2+}. The appearance of a clear isosbestic point at 393 nm and the slight increase in absorbance of the shoulder at approx. 422 nm indicates the formation of a new complex between Que and Fe^{2+} (the different molar ratios can be verified by the corresponding calibration curves in Fig.S4) in a similar fashion as previously described for native quercetin by Maolin Guo [36]. Considering that the major band at 370 nm in the UV-Vis spectrum of Que-2HP-β-CD complex comes from Que and originates from the cinnamoyl system between B+C rings, it can be assumed that Fe^{2+} chelates this particular binding site [49]. As shown in Fig. 7A and Fig. 7B the formation of the new complex is directly associated to the pH as hydrogen bonding is favored at physiological pH compared to the slightly acidic conditions [50, 51]. At physiological pH, one hydroxyl group at ring B is deprotonated to form anion A^- (curve j in Fig. 5 and Panel A in Figure S3), while at alkaline solutions the

second OH group at ring B can be deprotonated [10], thus the formation of metal complexes is favored at the catechol group.

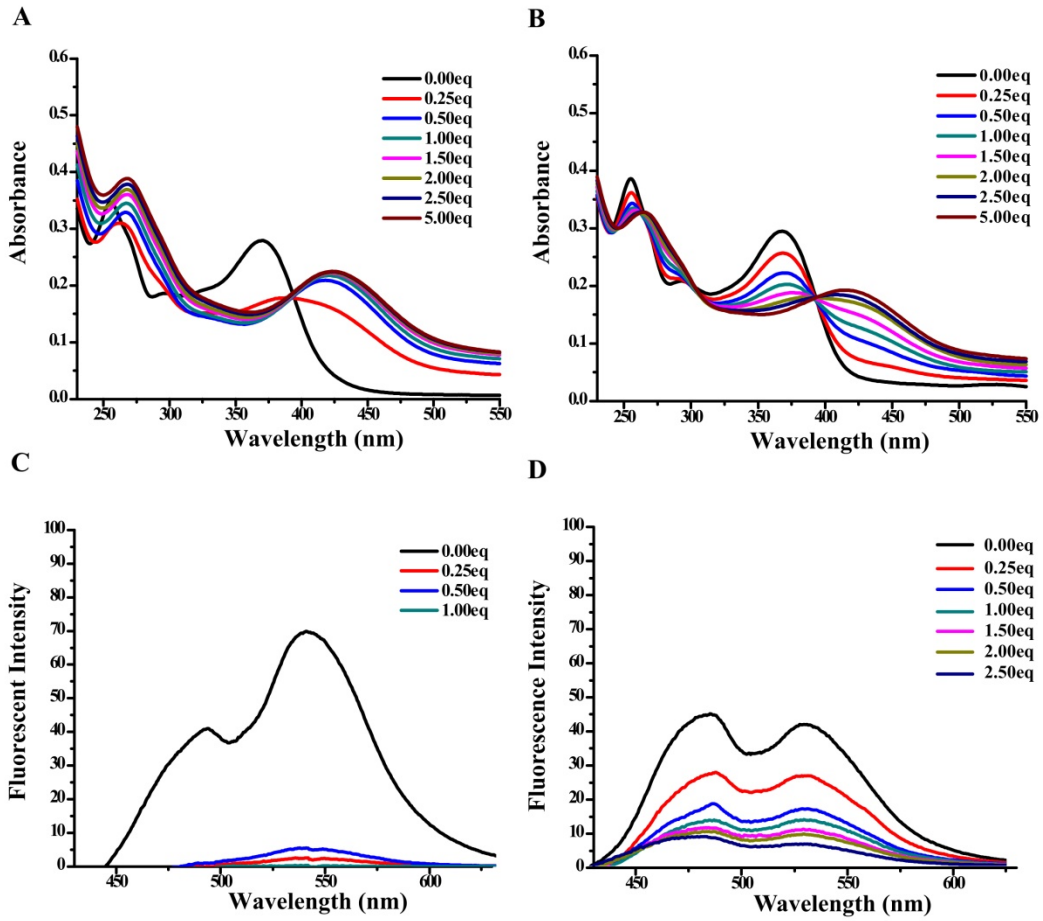

***Figure 7**: Absorption spectra of Que-2HP-β-CD (17 μM) in the presence of different concentrations of Fe^{2+} in H_2O at (A) pH 7.25 and (B) 5.81 respectively. Fluorescence spectra of Que 2HP-β-CD (17 μM) in the presence of different concentrations of Fe^{2+} in H_2O at (C) pH 7.25 and (D) 5.81, upon excitation at 370 nm.*

According to Simkovitch *et al*., the fluorescence spectrum of quercetin in aqueous solutions is consisted of two emission bands [51]. The first band exhibits a maximum at 440-470 nm and is assigned to the normal form of quercetin while the second band exhibits a maximum centered at 535 nm originated from its tautomeric form. The tautomeric form of quercetin is directly affected by pH and takes place via a proton transfer either from the 5-OH or the 3-OH position to the carbonyl group forming a six and a five membered ring, respectively [51]. As shown in Fig. 7C and Fig. 7D, the band intensity ratio is clearly highly dependent on the pH. At physiological pH the fluorescence intensity originated from the tautomeric form is

higher than the slightly acidic pH as the hydrogen bonding is favored [51]. In order to verify whether the complex between Fe^{2+} and Que retains the fluorescent intensity of native quercetin, further experiments were conducted. Upon titrating Fe^{2+}, the fluorescence intensity of Que-2HP-β-CD complex, upon excitation at 370 nm, was gradualy decreased. Concerning the turn off fluorescence mechanism it's possibe that the observed intensity quenching is a result of the energy transfer from quercetin to the empty d-orbitals of Fe^{2+} in a similar fashion as described for native quercetin by K. Kakavand *et al.* [52].

The binding affinity between Que 2HP-β-CD complex and Fe^{3+} was studied in a similar fashion. As shown in Fig. 8A and Fig. 8B the complexation between Que and Fe^{3+} at high pH requires less equivalents of Fe^{3+} as Que could exist in its deprotonated form favoring the formation of a complex, as indicated by the gradual appearance of a shoulder at 422 nm and the existence of an isosbestic point at appx. 394 nm. As the UV-Vis spectra changed in the same manner as in the case of Fe^{2+} it was assumed that the complexation takes place at the same binding site. In order to get a deeper understanding, fluorescence experiments were performed, and the results illustrated similar binding as in the case of Fe^{2+}. The gradual additions of more equivalents of Fe^{3+} lead to a significant precipitation, resulting a decrease of the absorbance at 422 nm. Of interest was that the observed dark yellow precipitate (color of quercetin) can potentially assigned to the decomplexation of quercetin.

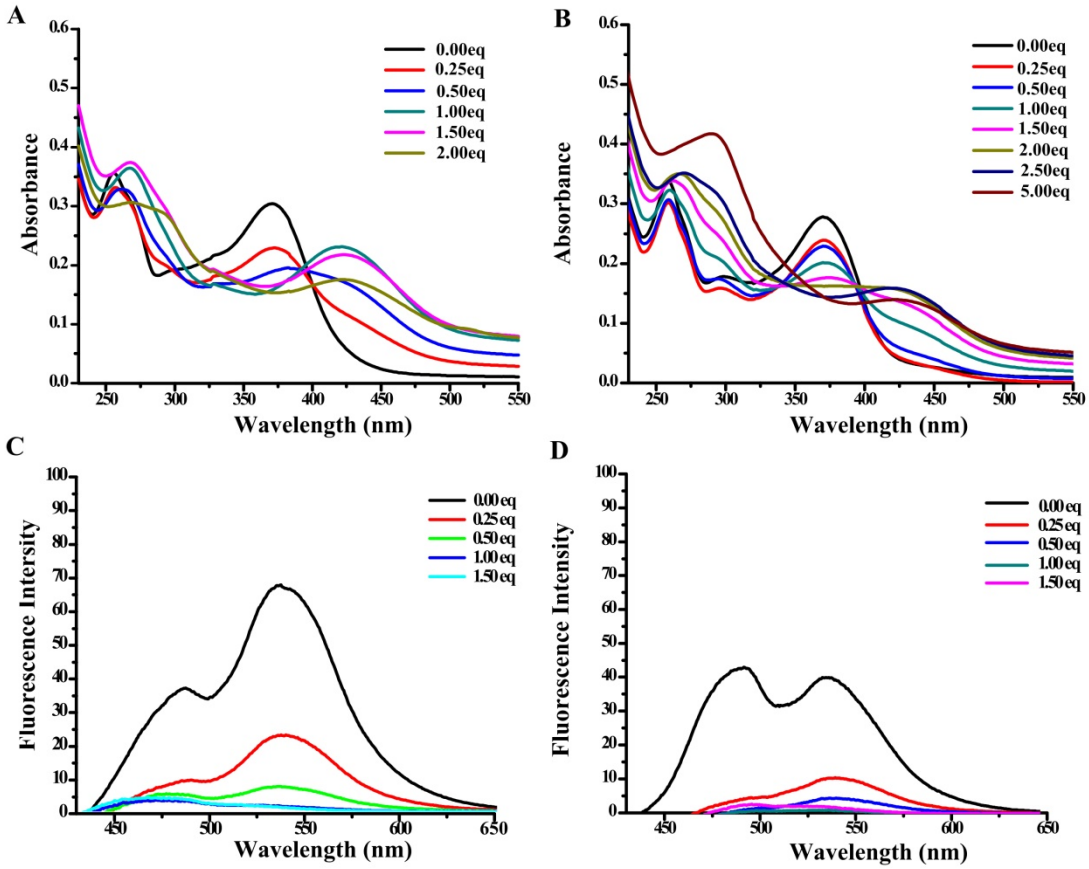

***Figure 8**: Absorption spectra of Que-2HP-β-CD (17 μM) in the presence of different concentrations of Fe^{3+} in H_2O at (A) pH 7.25 and (B) 5.81 respectively. Fluorescence spectra of Que 2HP-β-CD (17μM) in the presence of different concentrations of Fe^{3+} in H_2O at (C) pH 7.25 and (D) 5.81 respectively, upon excitation at 370 nm.*

In order to verify whether the iron species selectively bind quercetin or interact with cyclodextrin, NMR titrations were conducted both for Que 2HP-β-CD complex and native 2HP-β-CD in D_2O (pH=7.17). As shown in Fig.9, Que initially forms a metal complex with the paramagnetic Fe^{3+} ions, as it is clear from the extensive line width broadening and change in the chemical shift [53]. However, after the addition of 1.0 eq of Fe^{3+} precipitation was clearly observed. The mixture was centrifuged, and the precipitate was successively washed twice with H_2O (2*1 ml). Subsequently, the solid was redisssolved in DMSO-d_6 and the ^1H NMR spectrum revealed that it is native quercetin. Moreover, NMR titration was performed for native 2HP-β-CD with Fe^{3+} and it was found that 2HP-β-CD binds Fe^{3+} (Fig. S6) in a similar fashion as described by Halaszova *et al*. [54], so it can be assumed that two phenomena could

co-exist: iron triggers the un-loading/de-complexation of quercetin from 2HP-β-CD and this originates upon interaction of iron both with Que and 2HP-β-CD.

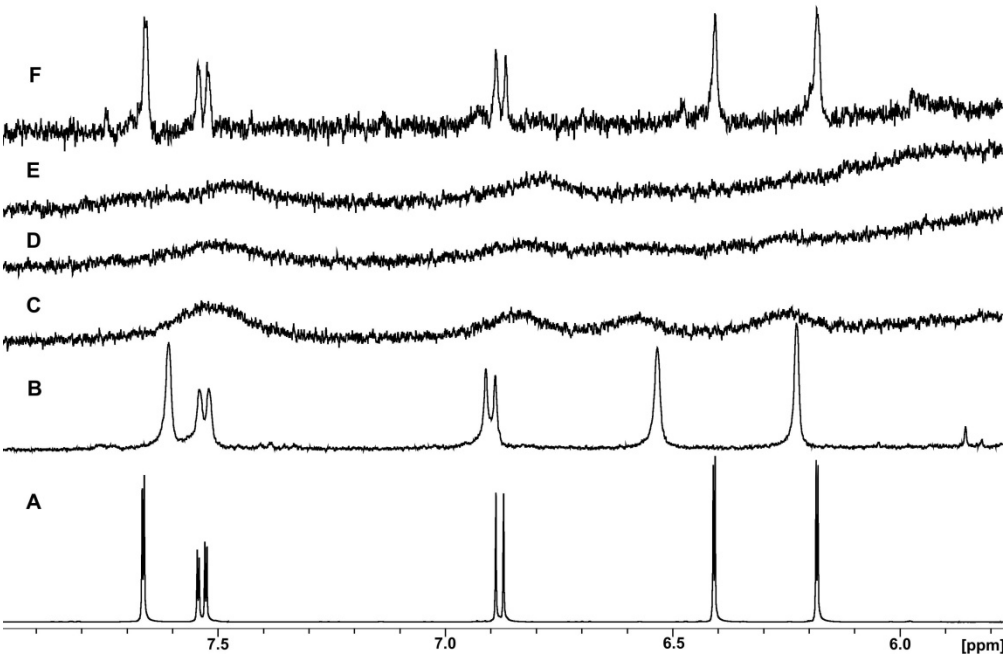

***Figure 9**: Selected region of the ^{1}H NMR spectra of: **A)** native Que in DMSO-d_6; **B)** Que-2HP-β-CD complex (3.8mM) in 100% D_2O; **C)** Que-2HP-β-CD complex (3.8mM) in D_2O after the addition of 0.25 eq. of Fe^{3+}. **D)** Que-2HP-β-CD complex (3.8mM) in D_2O after the addition of 0.50 eq. of Fe^{3+}; **E)** Que-2HP-β-CD complex (3.8mM) in D_2O after the addition of 1.0 eq. of Fe^{3+}; **F)** the observed precipitate in DMSO-d_6 after the addition of 1.0 eq. of Fe^{3+} in Que-2HP-β-CD complex (3.8mM).*

To conclude, iron species displayed similar alternation motif concerning the photophysical properties compare to the initial spectra of Que 2HP-β-CD. More specifically, it was observed that the UV-Vis spectra was red shifted to 422 nm while the fluorescence intensity was quenched, in a similar fashion as described for native quercetin by Maolin Guo *et al* and K. Kakavand *et al.* for UV-Vis and fluorescence titrations respectively, suggesting metal complexation with iron species [36] [52]. In the case of ferric iron, the resulting metal complex was insoluble in aqueous solution and precipitation could clearly observed compared to ferrous iron.

3.5 Evaluation of the protection offered by native quercetin and its encapsulated form against H_2O_2-induced DNA damage in living cells

The degree of DNA protection offered by different concentrations of native Que as also of its formulate with 2HP-β-CD, when added to cells for 20 min, before the exposure to H_2O_2, was evaluated in Jurkat cells by using the comet assay methodology, as previously reported for other phenolic compounds [40, 55]. As shown in Fig. 10A, preincubation of the cells with Que offered the highest protection at 80μM. On the contrary, the encapsulated form of Que in 2HP-β-CD did not offer considerable degree of DNA protection (Fig. 10B). A much lower protection is observed also at 80μM that could be potentially attributed to a dissociation of the complex. Based on our previous findings that compounds bearing the ortho-dihydroxyl moiety were able to chelate labile iron and thereby to prevent H_2O_2-induced DNA damage [40, 55], it was hypothesized that the low effectiveness of Que-2HP-β-CD was emanated from its inability to penetrate through plasma membrane due to the polar character of 2HP-β-CD.

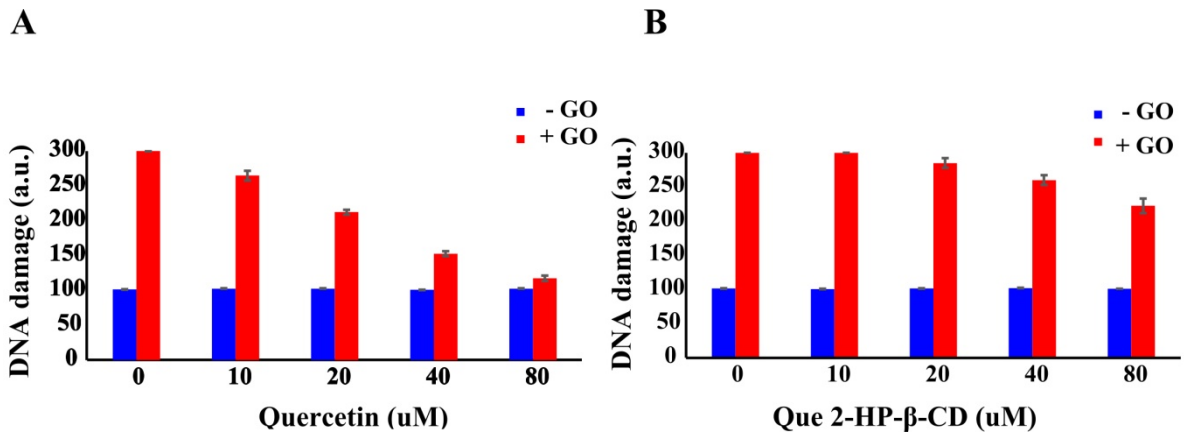

***Figure 10**: Protective effects offered by quercetin and the inclusion complex against H_2O_2-induced DNA damage. Jurkat cells in culture (1.5 × 10^6 cells/ml) were pre-incubated for 20 min with the indicated concentrations (0, 10, 20, 40, and 80 μM) of the quercetin (A) or the inclusion complex (B) and then exposed to an amount of glucose oxidase (0.6μg/ml) able to generate about 10 μM H_2O_2 per minute. After 10 min of exposure to H_2O_2, cells were collected and analyzed for formation of single-strand breaks in their DNA by using the comet assay methodology. DNA damage was expressed in arbitrary units (a.u.), as described under Materials and Methods. Each point represents the mean ± SD of duplicate measurements in two separate experiments.*

4. Conclusion

Herein, are utilized an array of biophysical techniques to unveil the oxidation profile, the aqueous solubility and rate of dissolution at a wide pH range indicated by the FDA and EMA regulations, the metal ion chelation properties as also the protection of DNA damage from ox-

idative stress of a flavonoid once it is encapsulated in a supramolecular cyclodextrin carrier. The enhanced aqueous solubility offered by the Que-2HP-β-CD complex, compared to the native compound, as well as the amplified dissolution of quercetin originated from the inclusion complex indicate increased bioavailability of the inclusion complex after oral administration. In the inclusion complex Que retained the same electrochemical oxidation profile of the native compound as also the ability to chelate iron species. We also revealed that iron species can operate as a chemical stimulus that can lead to a controlled release of the flavonoid from the host core. These results could pave the way to unleash the full biological potential and health benefits of a large reservoir of natural products that their bioactivity is largely depreciated due to their limited solubility.

Conflict of interest:

The authors declare no conflict of interest

References

[1] D.A. Dias, S. Urban, U. Roessner, A historical overview of natural products in drug discovery, Metabolites, 2 (2012) 303-336.

[2] D.J. Newman, G.M. Cragg, Natural Products as Sources of New Drugs from 1981 to 2014, Journal of Natural Products, 79 (2016) 629-661.

[3] M. Zahedi, R. Ghiasvand, A. Feizi, G. Asgari, L. Darvish, Does Quercetin Improve Cardiovascular Risk factors and Inflammatory Biomarkers in Women with Type 2 Diabetes: A Double-blind Randomized Controlled Clinical Trial, International journal of preventive medicine, 4 (2013) 777-785.

[4] H.P. Kim, I. Mani, L. Iversen, V.A. Ziboh, Effects of naturally-occurring flavonoids and biflavonoids on epidermal cyclooxygenase and lipoxygenase from guinea-pigs, Prostaglandins, leukotrienes, and essential fatty acids, 58 (1998) 17-24.

[5] S.F. Nabavi, G.L. Russo, M. Daglia, S.M. Nabavi, Role of quercetin as an alternative for obesity treatment: you are what you eat!, Food chemistry, 179 (2015) 305-310.

[6] S. Ramesova , R. Sokolova , I. Degano, M. Hromadova, M. Galz, V. Kolivoska, M.P. Colombini, The Influence of the Host-guest Interacation on the Oxidation of Natural Flavonoid Dyes, Collection of Czechoslovak Chemical Communications 76 (2011) 1651-1667

[7] Š. Ramešová, R. Sokolová, I. Degano, The study of the oxidation of the natural flavonol fisetin confirmed quercetin oxidation mechanism, Electrochimica Acta, 182 (2015) 544-549.

[8] R. Sokolová, Š. Ramešová, J. Kocábová, V. Kolivoška, I. Degano, E. Pitzalis, On the difference in decomposition of taxifolin and luteolin vs. fisetin and quercetin in aqueous media, Monatshefte für Chemie - Chemical Monthly, 147 (2016) 1375-1383.

[9] Š. Ramešová, I. Degano, R. Sokolová, The oxidative decomposition of natural bioactive compound rhamnetin, Journal of Electroanalytical Chemistry, 788 (2017) 125-130.

[10] R. Sokolova, S. Ramesova, I. Degano, M. Hromadova, M. Gal, J. Zabka, The oxidation of natural flavonoid quercetin, Chemical Communications, 48 (2012) 3433-3435.

[11] X. Cai, Z. Fang, J. Dou, A. Yu, G. Zhai, Bioavailability of quercetin: problems and promises, Current medicinal chemistry, 20 (2013) 2572-2582.
[12] I.M. Savic, V.D. Nikolic, I. Savic-Gajic, L.B. Nikolic, B.C. Radovanovic, J.D. Mladenovic, Investigation of properties and structural characterization of the quercetin inclusion complex with (2-hydroxypropyl)-β-cyclodextrin, Journal of Inclusion Phenomena and Macrocyclic Chemistry, 82 (2015) 383-394.
[13] C. Jullian, V. Brossard, I. Gonzalez, M. Alfaro, C. Olea-Azar, Cyclodextrins-Kaempferol Inclusion Complexes: Spectroscopic and Reactivity Studies, Journal of Solution Chemistry, 40 (2011) 727-739.
[14] P.J. Salustio, P. Pontes, C. Conduto, I. Sanches, C. Carvalho, J. Arrais, H.M. Marques, Advanced technologies for oral controlled release: cyclodextrins for oral controlled release, AAPS PharmSciTech, 12 (2011) 1276-1292.
[15] S. Das, U. Subuddhi, Cyclodextrin Mediated Controlled Release of Naproxen from pH-Sensitive Chitosan/Poly(Vinyl Alcohol) Hydrogels for Colon Targeted Delivery, Industrial & Engineering Chemistry Research, 52 (2013) 14192-14200.
[16] V.C. Barry, L. O'Rourke, D. Twomey, Antitubercular activity of diphenyl ethers and related compounds, Nature, 160 (1947) 800.
[17] E. Christodoulou, I.-A. Kechagia, S. Tzimas, E. Balafas, N. Kostomitsopoulos, H. Archontaki, A. Dokoumetzidis, G. Valsami, Serum and tissue pharmacokinetics of silibinin after per os and i.v. administration to mice as a HP-β-CD lyophilized product, International Journal of Pharmaceutics, 493 (2015) 366-373.
[18] T.F. Kellici, D. Ntountaniotis, G. Leonis, M. Chatziathanasiadou, A.V. Chatzikonstantinou, J. Becker-Baldus, C. Glaubitz, A.G. Tzakos, K. Viras, P. Chatzigeorgiou, S. Tzimas, E. Kefala, G. Valsami, H. Archontaki, M.G. Papadopoulos, T. Mavromoustakos, Investigation of the Interactions of Silibinin with 2-Hydroxypropyl-β-cyclodextrin through Biophysical Techniques and Computational Methods, Molecular Pharmaceutics, 12 (2015) 954-965.
[19] J. Liang, B. Liu, ROS-responsive drug delivery systems, Bioengineering & Translational Medicine, 1 (2016) 239-251.
[20] N.V. Roik, L.A. Belyakova, pH-Sensitive Supramolecular Assemblies of β-Cyclodextrin and 2-Aminodiphenylamine in Water Medium: Structure, Solubility and Stability, Journal of Solution Chemistry, 45 (2016) 818-830.
[21] P.J. Salústio, P. Pontes, C. Conduto, I. Sanches, C. Carvalho, J. Arrais, H.M.C. Marques, Advanced Technologies for Oral Controlled Release: Cyclodextrins for Oral Controlled Release, AAPS PharmSciTech, 12 (2011) 1276-1292.
[22] T. Nakamura, Y. Takashima, A. Hashidzume, H. Yamaguchi, A. Harada, A metal-ion-responsive adhesive material via switching of molecular recognition properties, Nature communications, 5 (2014) 4622.
[23] T.F. Kellici, M.V. Chatziathanasiadou, D. Diamantis, A.V. Chatzikonstantinou, I. Andreadelis, E. Christodoulou, G. Valsami, T. Mavromoustakos, A.G. Tzakos, Mapping the interactions and bioactivity of quercetin—(2-hydroxypropyl)-β-cyclodextrin complex, International Journal of Pharmaceutics, 511 (2016) 303-311.
[24] EMA Guideline on the Investigation of Bioequivalence, CPMP/EWP/QWP/1401/98 Rev. 1/Corr**, London, 20 January 2010 .
[25] Waiver of In Vivo Bioavailability and Bioequivalence Studies for Immediate-Release Solid Oral Dosage Forms Based on a Biopharmaceutics Classification System Guidance for Industry, (2017).
[26] M. Krejčik, M. Daněk, F. Hartl, Simple construction of an infrared optically transparent thin-layer electrochemical cell, Journal of Electroanalytical Chemistry and Interfacial Electrochemistry, 317 (1991) 179-187.
[27] N.P. Singh, M.T. McCoy, R.R. Tice, E.L. Schneider, A simple technique for quantitation of low levels of DNA damage in individual cells, Exp Cell Res, 175 (1988) 184-191.

[28] M. Panayiotidis, O. Tsolas, D. Galaris, Glucose oxidase-produced H2O2 induces Ca2+-dependent DNA damage in human peripheral blood lymphocytes, Free Radic Biol Med, 26 (1999) 548-556.
[29] P. Macheras, V. Karalis, G. Valsami, Keeping a critical eye on the science and the regulation of oral drug absorption: A review, Journal of Pharmaceutical Sciences, 102 (2013) 3018-3036.
[30] L.X. Yu, G.L. Amidon, J.E. Polli, H. Zhao, M.U. Mehta, D.P. Conner, V.P. Shah, L.J. Lesko, M.L. Chen, V.H. Lee, A.S. Hussain, Biopharmaceutics classification system: the scientific basis for biowaiver extensions, Pharm Res, 19 (2002) 921-925.
[31] R. Löbenberg, J. Krämer, V.P. Shah, G.L. Amidon, J.B. Dressman, Dissolution Testing as a Prognostic Tool for Oral Drug Absorption: Dissolution Behavior of Glibenclamide, Pharmaceutical Research, 17 (2000) 439-444.
[32] D. Riethorst, R. Mols, G. Duchateau, J. Tack, J. Brouwers, P. Augustijns, Characterization of Human Duodenal Fluids in Fasted and Fed State Conditions, Journal of Pharmaceutical Sciences, 105 673-681.
[33] S.-G. Wu, J.-Y. Shih, Management of acquired resistance to EGFR TKI–targeted therapy in advanced non-small cell lung cancer, Molecular Cancer, 17 (2018) 38.
[34] S. Waldmann, M. Almukainzi, N.A. Bou-Chacra, G.L. Amidon, B.-J. Lee, J. Feng, I. Kanfer, J.Z. Zuo, H. Wei, M.B. Bolger, R. Löbenberg, Provisional Biopharmaceutical Classification of Some Common Herbs Used in Western Medicine, Molecular Pharmaceutics, 9 (2012) 815-822.
[35] R.K. Verbeeck, F.T. Musuamba, The revised EMA guideline for the investigation of bioequivalence for immediate release oral formulations with systemic action, J Pharm Pharm Sci, 15 (2012) 376-388.
[36] M. Guo, C. Perez, Y. Wei, E. Rapoza, G. Su, F. Bou-Abdallah, N.D. Chasteen, Iron-binding properties of plant phenolics and cranberry's bio-effects, Dalton Transactions, (2007) 4951-4961.
[37] G. Jungbluth, I. Ruhling, W. Ternes, Oxidation of flavonols with Cu(II), Fe(II) and Fe(III) in aqueous media, Journal of the Chemical Society, Perkin Transactions 2, (2000) 1946-1952.
[38] O. Dangles, G. Fargeix, C. Dufour, One-electron oxidation of quercetin and quercetin derivatives in protic and non protic media, Journal of the Chemical Society, Perkin Transactions 2, (1999) 1387-1396.
[39] D. Galaris, K. Pantopoulos, Oxidative stress and iron homeostasis: mechanistic and health aspects, Critical reviews in clinical laboratory sciences, 45 (2008) 1-23.
[40] N. Kitsati, M.D. Mantzaris, D. Galaris, Hydroxytyrosol inhibits hydrogen peroxide-induced apoptotic signaling via labile iron chelation, Redox biology, 10 (2016) 233-242.
[41] P.S. Gerogianni, M.V. Chatziathanasiadou, D.A. Diamantis, A.G. Tzakos, D. Galaris, Lipophilic ester and amide derivatives of rosmarinic acid protect cells against H2O2-induced DNA damage and apoptosis: The potential role of intracellular accumulation and labile iron chelation, Redox biology, 15 (2018) 548-556.
[42] S. Yang, B. Yin, L. Xu, B. Gao, H. Sun, L. Du, Y. Tang, W. Jiang, F. Cao, A natural quercetin-based fluorescent sensor for highly sensitive and selective detection of copper ions, Analytical Methods, 7 (2015) 4546-4551.
[43] Y. Liu, M. Guo, Studies on Transition Metal-Quercetin Complexes Using Electrospray Ionization Tandem Mass Spectrometry, Molecules, 20 (2015).
[44] R. Ravichandran, M. Rajendran, D. Devapiriam, Antioxidant study of quercetin and their metal complex and determination of stability constant by spectrophotometry method, Food chemistry, 146 (2014) 472-478.
[45] D. Zhong, M. Liu, Y. Cao, Y. Zhu, S. Bian, J. Zhou, F. Wu, K.-C. Ryu, L. Zhou, D. Ye, Discovery of Metal Ions Chelator Quercetin Derivatives with Potent Anti-HCV Activities, Molecules, 20 (2015).
[46] M.M. Kasprzak, A. Erxleben, J. Ochocki, Properties and applications of flavonoid metal complexes, RSC Advances, 5 (2015) 45853-45877.

[47] L. Mira, M.T. Fernandez, M. Santos, R. Rocha, M.H. Florencio, K.R. Jennings, Interactions of flavonoids with iron and copper ions: a mechanism for their antioxidant activity, Free radical research, 36 (2002) 1199-1208.
[48] J.M. Dimitric Markovic, Z.S. Markovic, T.P. Brdaric, N.D. Filipovic, Comparative spectroscopic and mechanistic study of chelation properties of fisetin with iron in aqueous buffered solutions. Implications on in vitroantioxidant activity, Dalton Transactions, 40 (2011) 4560-4571.
[49] M. Massaro, S. Piana, C.G. Colletti, R. Noto, S. Riela, C. Baiamonte, C. Giordano, G. Pizzolanti, G. Cavallaro, S. Milioto, G. Lazzara, Multicavity halloysite-amphiphilic cyclodextrin hybrids for co-delivery of natural drugs into thyroid cancer cells, Journal of Materials Chemistry B, 3 (2015) 4074-4081.
[50] K. Lemanska, H. Szymusiak, B. Tyrakowska, R. Zielinski, A.E. Soffers, I.M. Rietjens, The influence of pH on antioxidant properties and the mechanism of antioxidant action of hydroxyflavones, Free Radic Biol Med, 31 (2001) 869-881.
[51] R. Simkovitch, D. Huppert, Excited-State Intramolecular Proton Transfer of the Natural Product Quercetin, The journal of physical chemistry. B, 119 (2015) 10244-10251.
[52] V.N. K. Kakavand, F. Faridbod, H. Ebrahimzadeh, A. Hamidipour Interaction study of a secondary metabolite quercetin with metal ions by conductometry and fluorescence spectroscopy, Analytical and Bioanalytical Electrochemistry, 4 (2012) 635-645.
[53] C.L. I. Bertini, G. Parigi, E. Ravera, NMR of Paramagnetic Molecules (Second Edition) Applications to Metallobiomolecules and Models, in, vol. 2, Elsevier, 2016.
[54] S. Halaszova, M. Jerigova, D. Lorenc, D. Velic, Preparation of Cyclodextrin-Iron Species in Water by Laser Ablation: Secondary Ion Mass Spectrometry, Chemphyschem : a European journal of chemical physics and physical chemistry, 16 (2015) 2110-2113.
[55] M. Melidou, K. Riganakos, D. Galaris, Protection against nuclear DNA damage offered by flavonoids in cells exposed to hydrogen peroxide: the role of iron chelation, Free Radic Biol Med, 39 (2005) 1591-1600.